Observation of Multichannel Collisions of Cold Metastable Calcium Atoms

Dirk Hansen* and Andreas Hemmerich

Institut für Laser-Physik, Universität Hamburg, Luruper Chaussee 149, 22761 Hamburg, Germany

(Received 5 October 2005; published 24 February 2006)

Recent theoretical work indicates that collisions between metastable alkaline-earth atoms (AEAs) in the presence of external magnetic fields should be largely determined by partial waves with large angular momenta even at very low temperatures. Unusually large inelastic collision cross sections were predicted and doubts have been raised regarding the feasibility of evaporative cooling of metastable AEAs in magnetic traps. Here we present experimental data for ^{40}Ca$[4s4p]^3P_2$ clearly confirming the asserted multichannel character of the collision mechanism. While elastic cross sections are found to be similar to the predicted values, inelastic cross sections exceed the calculations by an order of magnitude. Our results substantiate the expectation of inefficient evaporative cooling.

DOI: 10.1103/PhysRevLett.96.073003 PACS numbers: 34.50.−s, 32.80.Pj, 82.20.Pm

Substantial progress in laser cooling of alkaline-earth atoms (AEAs) [1–5] has opened up a new exciting test ground to confront advanced collision theory with precise experiments at low temperatures [6–11]. The absence of hyperfine structure for bosonic AEAs reduces computational complexity, while at the same time the tiny anisotropy of the collision potentials in the long-lived metastable $^3P_2$ state in the presence of an external magnetic field allows one to examine collision theory at ultralow temperatures well beyond the S-wave approximation. Because of their unique electronic properties, AEAs are also at the focus of other rapidly evolving lines of research in atomic physics. The most prominent examples are the fields of quantum gases [12,13] and time metrology [14]. In both cases, the application of AEAs may yield fundamentally new developments. Sufficiently cold and dense ensembles of metastable AEAs could be used as an inverted medium for matter wave amplification by optical pumping [15–17]. The large g factor of the $^3P_2$ state gives rise to a dipolar magnetic interaction, which could become visible in a $^3P_2$-Bose-Einstein condensate (BEC) and may thus provide us with a new system for exploring polar quantum fluids [18,19]. Ultranarrow intercombination transitions available in AEAs are prime candidates to serve as optical balance wheels in next generation atomic clocks bearing the promise of unprecedented precision [20–26]. These exciting perspectives, however, crucially rely on knowing, understanding, and possibly controlling [11] the collisional properties of metastable AEAs.

Recently, in two pioneering articles, the multichannel character of binary collisions in the $^3P_2$ state has been theoretically explored for the cases of strontium and calcium [9,10]. In Ref. [10], it was shown that partial waves with large angular momenta L strongly modify the $^3P_2$ elastic collision cross sections even at microkelvin temperatures. Inelastic collision cross sections of spin-polarized samples ($^3P_2$, $m = 2$) were shown to be dominated by partial waves with $L > 6$. Predictions of the collision cross sections were made, significantly exceeding those of typical alkaline systems. It was suspected that the standard magnetic trapping approach for preparation of a BEC of $^3P_2$, $m = 2$ AEAs is inappropriate because of an unfavorable ratio between elastic and inelastic collision rates, which yields excessive particle loss and prevents evaporative cooling.

In this Letter, we present the, to our knowledge, first experimental study of the collisional properties of metastable AEAs. We examine ^{40}Ca atoms in the $^3P_2$, $m = 2$ state (denoted as Ca* in the following), confined in a miniaturized magnetic trap, and confront our observations with the theory of Ref. [10]. We measure comparable values (around 3×10^{-10} cm^3 s^{-1}) for elastic and inelastic collision parameters, largely independent of the temperature or the magnetic field. This definitely excludes the possibility of evaporative cooling in magnetic traps for Ca*, a fact that should apply to other metastable AEAs as well. Attempts towards BEC of Ca* (and most probably also of Sr*) should thus resort to trapping techniques using the lowest energy component of the $^3P_2$ manifold, in order to inhibit inelastic collisions. The observed elastic collision parameter exceeds the unitarity limit of S-wave scattering by a factor of 10, thus clearly demonstrating that, despite the low temperatures of a few hundred microkelvin, the collision mechanism involves partial waves with large angular momenta. Quantitatively, our findings for magnetic fields varying between 2 and 10 Gauss exceed the theoretical predictions made for slightly larger magnetic fields (100 Gauss) by a factor of 2 in the case of the elastic cross section and surprisingly by more than an order of magnitude for the inelastic cross section. This indicates that, particularly at low magnetic field values, aside from the long-range mechanism described in Ref. [10], other contributions, possibly due to short-range molecular potentials, need to be accounted for. An open question is the potential role of fine-structure changing collisions. We believe that this work will stimulate further theoretical efforts to bridge the present gap between experiment and theory, which would be highly desirable in view of the persisting interest in quantum degenerate Ca* and Sr*.

In the experiment, samples of several 10^8 Ca^* atoms are provided by a bichromatic magneto-optic trap as described in Ref. [4]. The atoms are magnetically conveyed over a distance of 26 mm to three (millimeter-sized) solenoids arranged in a quadrupole Ioffe configuration (QUIC), thus providing a magnetic trap with a nonzero bias field [cf. Fig. 1(a)] [27]. For optimal atom transfer, the QUIC trap initially operates with a bias field of 16 G and a shallow magnetic field curvature. In a second step, the desired trapping parameters are adjusted adiabatically. We use a final trap geometry with nearly axial symmetry and with an aspect ratio between the axial [z axis in Fig. 1(a)] and radial [xy plane in Fig. 1(a)] magnetic field curvatures of 2.24 and a fixed ratio of 0.3 mm^2 between the bias field and the axial magnetic field curvature. With 20 W of heat dissipation in the magnetic coils, we achieve trap frequencies $\nu_{\mathrm{rad}} \equiv \nu_x \approx \nu_y = 300$ Hz, $\nu_{\mathrm{ax}} \equiv \nu_z = 130$ Hz. By adiabatic variation of the magnetic field curvature, temperatures ranging from a few hundred microkelvin to a few millikelvin are adjusted. The accessible temperature range is extended by a preceding Doppler-cooling phase [28–31]. The atoms are irradiated by two counterpropagating σ_+ polarized laser beams oriented along the symmetry axis of the trap [z axis in Fig. 1(a)] and slightly detuned to the red side of the $^3P_2$, $m = 2 \rightarrow {}^3D_3$, $m = 3$ transition at 1978 nm [see Fig. 1(b)]. The 16 G magnetic bias field provides the required frequency selectivity with respect to different Zeeman components [30]. All relevant information on the atomic sample is obtained by absorption images along the x axis [Fig. 1(a)]. A short pulse of 430 nm light optically pumps the atoms to the magnetically insensitive singlet ground state [via the short-lived (0.3 ms) $^3P_1$ state], where an absorption image is obtained by means of the closed cycle transition at 423 nm (cf. Fig. 1). For pulse durations exceeding 20 μs, the $^3P_2$ state is completely depopulated.

Elastic binary collision rates are investigated via cross-dimensional relaxation measurements [31–34]. By means of Doppler cooling and adiabatic adjustment of the trap well depth, different initial temperatures T_{ax} and T_{rad} in the axial and radial directions are prepared. Thermalization due to elastic collisions and ergodic mixing bring the sample back to equilibrium. The resulting change of the aspect ratio $A(t)$ between the axial and radial diameters of the atomic spatial distribution is measured in the experiment. Extending the model used in Refs. [31,33,34], we describe the relaxation of $A(t)$ towards its equilibrium value A_{eq} by

$$\frac{d}{dt}A(t) = -\gamma_{\mathrm{rel}}(t)(A(t) - A_{\mathrm{eq}}). \tag{1}$$

The relaxation rate $\gamma_{\mathrm{rel}}(t) \equiv \gamma_{\mathrm{erg}} + \beta_{\mathrm{rel}}(t)\bar{n}(t)$ may slowly vary with time [$\frac{d}{dt}\gamma_{\mathrm{rel}}(t) \ll \gamma_{\mathrm{rel}}(t)^2$] to account for heating and particle loss. Here γ_{erg} is a constant rate describing ergodic mixing, the cross-dimensional relaxation parameter $\beta_{\mathrm{rel}}(t) \equiv \sigma_{\mathrm{rel}}(\bar{T}(t))\bar{v}(t)$ accounts for elastic binary collisions with a relaxation cross section $\sigma_{\mathrm{rel}}(\bar{T}(t))$, $\bar{v}(t)$ is the mean velocity in the atomic sample connected to the mean temperature $\bar{T}(t) \equiv (T_{\mathrm{ax}}(t) + 2T_{\mathrm{rad}}(t))/3$ according to $\bar{v} = (8k_B\bar{T}/\pi m)^{1/2}$ ($m \equiv$ atomic mass, $k_B \equiv$ Boltzmann constant), and $\bar{n}(t)$ denotes the mean number density derived from the number density distribution $n(r)$ according to $\bar{n}(t) \equiv \int n(r)^2 d^3r / \int n(r) d^3r$. We define scaled quantities and formally integrate Eq. (1) according to

$$A^*(t) \equiv \frac{1}{t}\ln\left(\frac{A(t) - A_{\mathrm{eq}}}{A(0) - A_{\mathrm{eq}}}\right), \qquad n_v^*(t) \equiv \frac{1}{t}\int_0^t \bar{n}(s)\frac{\bar{v}(s)}{\bar{v}(0)}ds,$$
$$A^*(t) = -\gamma_{\mathrm{erg}} - \beta_{\mathrm{rel}}(0)n_v^*(t). \tag{2}$$

Here it is assumed that the variation of $\sigma_{\mathrm{rel}}(\bar{T}(t))$ during the relaxation process due to heating may be neglected. Provided that the relaxation model of Eq. (1) is correct, by plotting $A(t)^*$ versus $n_v^*(t)$, one may obtain γ_{erg} and $\beta_{\mathrm{rel}}(0)$ as the y-axis intercept and the slope of a linear best fit to the data without making any additional assumptions about heating and trap loss. To this end, $A^*(t)$ and $n_v^*(t)$ are derived as follows. The optical density $D(y, z) \equiv \sigma \int n(r)dx$ along the x direction is measured by means of absorption imaging (σ denotes the resonant photon scattering cross section). The total number of particles is obtained by integrating $D(y, z)$ in the yz plane. The number density distribution $n(r)$ is derived upon the assumption of a Gaussian spatial distribution along the x direction. The mean number density $\bar{n}(t)$ is calculated from $n(r)$ by evaluating the corresponding integral. The temperatures $T_{\mathrm{ax}}(t)$ and $T_{\mathrm{rad}}(t)$, required to determine $n_v^*(t)$, are obtained from the observed sample radii σ_i in connection with the known trap oscillation frequencies according to $2m(\pi\nu_i\sigma_i)^2 = k_BT_i$, with $i \in \{\mathrm{ax}, \mathrm{rad}\}$. The scaled aspect ratio $A^*(t)$ is directly calculated from the measured values of $A(t)$.

In Fig. 2(a), we show a typical plot of $A^*(t)$ versus $n_v^*(t)$. The data are well approximated by a straight line nearly crossing the origin. This shows that the model of Eq. (2) provides the appropriate description of our data with a negligible ergodic mixing rate. In Fig. 2(b), the values of $\beta_{\mathrm{rel}}(0)$ are plotted for different initial mean temperatures $\bar{T}(0)$. The error budget aside from statistical errors includes a conservative account of systematic uncertainties. By far, the leading contributions are 10% uncertainty in the deter-

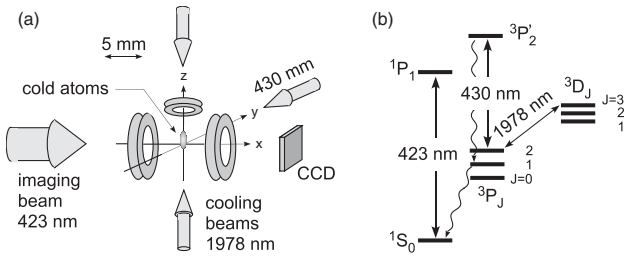

FIG. 1. (a) Sketch of the experiment. (b) Relevant levels and transitions of calcium.

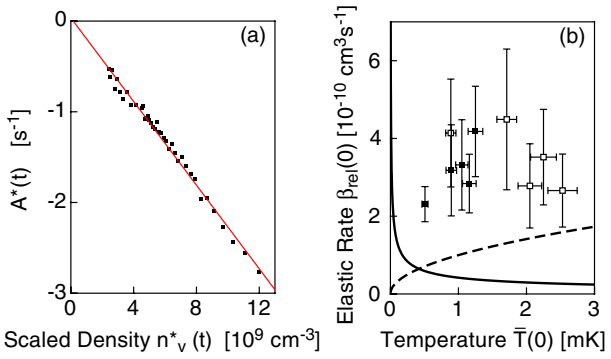

FIG. 2 (color online). (a) Observation of cross-dimensional relaxation. The scaled quantities of Eq. (2) are plotted and modeled by a linear fit (solid line). (b) Elastic relaxation parameter $\beta_{\mathrm{rel}}(0)$ plotted versus the initial mean temperature $\bar{T}(0)$. Solid (open) rectangles correspond to runs involving a (no) Doppler-cooling phase. The magnetic offset field varies between 2 and 10 Gauss. The dashed line is derived from the theory of Ref. [10] for a magnetic field of 100 Gauss; the solid line shows the unitarity limit for S-wave scattering.

mination of each of the following parameters: the aspect ratio $A(t)$, its equilibrium value A_{eq}, the sample size along the x direction (the line of sight for absorption imaging), and the optical density. The dashed line is derived from the theory of Ref. [10], which predicts an energy independent elastic scattering cross section $\sigma_{\mathrm{el}} = 2.4 \times 10^{-12}$ cm^2 for the respective temperature range. The solid line shows the unitarity limit for S-wave scattering, corresponding to an elastic scattering cross section $\sigma_{\mathrm{el}}(u) = 32\pi\hbar^2/(mu)^2$, where u denotes the relative velocity of the colliding atoms. For both cases, the corresponding elastic cross-dimensional relaxation coefficient β_{rel} has been calculated using Eqs. (73) and (79) of Ref. [35]. These equations employ an adapted thermal average which accounts for the fact that large relative velocities yield increased contributions to the cross-dimensional relaxation process. The measured values of β_{rel} are far too large in order to be explained by S-wave scattering, thus indicating that higher partial waves should play a dominant role. This nicely reflects the respective prediction of Ref. [10]. Nevertheless, the observations show that the calculation of Ref. [10] slightly underestimates elastic scattering, possibly because short-range molecular dynamics has not been accounted for.

The rate for binary inelastic collisions is determined by analyzing the loss of atoms from the trap. The number of atoms $N(t)$ confined within the effective trap volume $V_{\mathrm{eff}}(t) \equiv N(t)/\bar{n}(t)$ evolves according to

$$\frac{d}{dt}N(t) = -\gamma N(t) - \beta(t)\frac{N(t)^2}{V_{\mathrm{eff}}(t)}, \qquad (3)$$

with γ being the linear loss rate due to background gas collisions and $\beta(t) \equiv \sigma_{\mathrm{inel}}(\bar{T}(t))\bar{v}(t)$ denoting the two-body loss parameter, accounting for inelastic binary collisions. Assuming that each inelastic collision yields loss of both collision partners, we may directly identify $\sigma_{\mathrm{inel}}(\bar{T})$ with the cross section for inelastic collisions at temperature $\bar{T}$. Note that $\beta(t)$ and $V_{\mathrm{eff}}(t)$ may change in time due to heating of the sample, which results because inelastic losses occur predominantly at high density in the trap center where the coldest atoms reside. Slightly modifying the method used in Ref. [31], we can get around making assumptions regarding the peculiarities of the heating by employing scaled quantities and formally integrating Eq. (3) according to

$$N^*(t) \equiv \frac{1}{t}\ln\left(\frac{N(t)}{N(0)}\right), \qquad N^*(t) = -\gamma - \beta(0)n_v^*(t). \quad (4)$$

Similarly to Eq. (2), we have assumed here that the temperature change during the particle loss does not significantly alter $\sigma_{\mathrm{inel}}(\bar{T})$. Plotting the experimentally derived values $N^*(t)$ versus $n_v^*(t)$, the trap loss model in Eq. (3) predicts a straight line with y-axis intercept γ and slope $\beta(0)$.

A typical set of trap loss data plotted according to Eq. (4) is shown in Fig. 3(a). In Fig. 3(b), $\beta(0)$ is plotted for different mean temperatures realized in traps with different curvatures. While systematic errors concerning the temperature axis are comparable to those in Fig. 2(b), errors of $\beta(0)$ remain comparably small because uncertainties in the sample size play a far less significant role here. We observe slightly lower values of $\beta(0)$ if the preparation of atoms involves a Doppler-cooling phase [solid rectangles in Fig. 3(b)]. This reflects the fact that collisions involving $m = 1$ atoms are expected to exhibit larger cross sections than those between $m = 2$ atoms [10]. The atom samples become slightly depolarized during the (several hundred milliseconds long) magnetic transfer and, thus, comprise a small fraction of $m = 1$ atoms. The circularly polarized

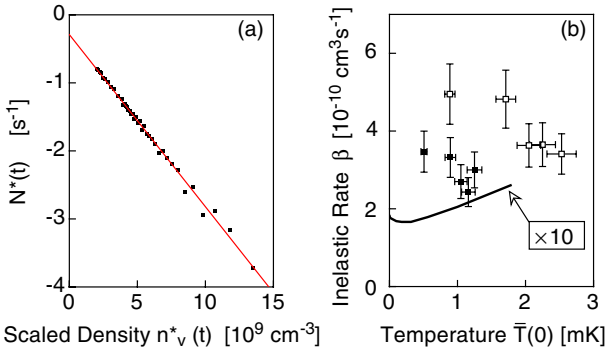

FIG. 3 (color online). (a) Observation of trap loss. The scaled quantities $N^*(t)$ and $n_v^*(t)$ defined in Eqs. (2) and (4) are plotted and modeled by a linear fit (solid line). (b) Loss parameter $\beta(0)$ plotted versus the mean temperature $\bar{T}(0)$. The magnetic offset field varied between 2 and 10 Gauss. Solid (open) rectangles correspond to runs involving a (no) Doppler-cooling phase. The solid line shows the calculations of Ref. [10] for 100 Gauss, multiplied by a factor ten.

Doppler-cooling beams, tuned to the red side of the $^3P_2$, $m = 2 \rightarrow {}^3D_3$, $m = 3$ transition, are also near resonant with respect to the $^3P_2$, $m = 1 \rightarrow {}^3D_3$, $m = 2$ transition. This gives rise to efficient optical pumping into the $^3P_2$, $m = 2$ level, which restores complete spin polarization. The solid line in Fig. 3(b) repeats the total inelastic rate of Fig. 3 in Ref. [10] calculated for $B = 100$ Gauss (multiplied by a factor of 10), which is given as a function of the relative incident kinetic energy specified in degrees Kelvin. Although no thermal average has been applied here, because the calculations accessible to us do not extend above kinetic energies of 1.8 K, a direct comparison with $\beta(0)$ appears appropriate since the dependence on kinetic energy is only marginal.

In conclusion, we have measured the two-body loss parameter for inelastic collisions and the cross-dimensional relaxation parameter due to elastic collisions of cold spin-polarized metastable calcium atoms (Ca^*) confined in a magnetic trap with a variable magnetic offset field (2–10 Gauss). We find similar exceptionally large values for both parameters, exceeding those predicted for slightly larger magnetic field values (100 Gauss) by the seminal calculations of Ref. [10]. The elastic scattering cross section is found to be much larger than the unitarity limit for S-wave scattering, thus confirming the asserted multichannel character of the collision mechanism. As a direct experimental consequence of this work, evaporative cooling is expected to fail for magnetically trapped Ca^*. In fact, we have applied resonant radio frequency, thus selectively removing energetic atoms from the trap. However, no increase of the phase space density could be obtained. Hence, Bose-Einstein condensation of Ca^* requires nonmagnetic trapping techniques, for example, the use of optical dipole traps. Ca^* as well as other AEAs appear to be ideal test systems for confronting advanced collision theory with experiments. Cold collision physics beyond S-wave scattering can be studied in a regime where computational complexity is significantly reduced due to the absence of hyperfine structure. With this in mind, we believe that our work will stimulate further theoretical efforts to bridge the present gap between theory and experiment. It should be an interesting challenge to include short-range molecular potentials in the calculations and account for fine-structure changing collisions. A quantitative theory on collisional properties of metastable AEAs is highly desirable in order to make this atom group accessible for the field of quantum gases as well as for controlling collisional line shifts of intercombination transitions presently considered to serve as a time base in future atomic clocks.

We gratefully acknowledge financial support by the DFG (*priority program SPP 1116*). We thank V. Kokoouline, R. Santra, and C. Greene for communicating their unpublished results on calcium. We also acknowledge notable technical support by C. Zafiu.

*Electronic address: dhansen@physnet.uni-hamburg.de

[1] H. Katori *et al.*, Phys. Rev. Lett. **82**, 1116 (1999).
[2] T. Binnewies *et al.*, Phys. Rev. Lett. **87**, 123002 (2001).
[3] E. Curtis *et al.*, Phys. Rev. A **64**, 031403(R) (2001).
[4] J. Grünert and A. Hemmerich, Phys. Rev. A **65**, 041401(R) (2002).
[5] T. H. Loftus *et al.*, Phys. Rev. Lett. **93**, 073003 (2004).
[6] T. P. Dinneen *et al.*, Phys. Rev. A **59**, 1216 (1999).
[7] J. Weiner *et al.*, Rev. Mod. Phys. **71**, 1 (1999).
[8] M. Machholm, P. S. Julienne, and K.-A. Suominen, Phys. Rev. A **65**, 023401 (2002).
[9] A. Derevianko *et al.*, Phys. Rev. Lett. **90**, 063002 (2003).
[10] V. Kokoouline, R. Santra, and C. Greene, Phys. Rev. Lett. **90**, 253201 (2003); the authors have communicated to us unpublished analog results for Ca.
[11] R. Ciurylo, E. Tiesinga, and P. S. Julienne, Phys. Rev. A **71**, 030701(R) (2005).
[12] K. Burnett *et al.*, Nature (London) **416**, 225 (2002).
[13] J. Anglin and W. Ketterle, Nature (London) **416**, 211 (2002).
[14] S. A. Diddams *et al.*, Science **306**, 1318 (2004).
[15] U. Janicke and M. Wilkens, Adv. At. Mol. Opt. Phys. **4**, 261 (1999).
[16] J. Grünert *et al.*, J. Mod. Opt. **47**, 2733 (2000).
[17] L. Santos *et al.*, Phys. Rev. A **63**, 063408 (2001).
[18] J. Doyle *et al.*, Eur. Phys. J. D **31**, 149 (2004), and following articles.
[19] J. Stuhler *et al.*, Phys. Rev. Lett. **95**, 150406 (2005).
[20] F. Ruschewitz *et al.*, Phys. Rev. Lett. **80**, 3173 (1998).
[21] G. Wilpers *et al.*, Phys. Rev. Lett. **89**, 230801 (2002).
[22] I. Courtillot *et al.*, Phys. Rev. A **68**, 030501(R) (2003).
[23] H. Katori *et al.*, Phys. Rev. Lett. **91**, 173005 (2003).
[24] S. G. Porsev *et al.*, Phys. Rev. A **69**, 021403(R) (2004).
[25] T. Ido *et al.*, Phys. Rev. Lett. **94**, 153001 (2005).
[26] C. W. Hoyt *et al.*, Phys. Rev. Lett. **95**, 083003 (2005).
[27] T. Esslinger *et al.*, Phys. Rev. A **58**, R2664 (1998).
[28] T. Hijmans *et al.*, J. Opt. Soc. Am. B **6**, 2235 (1989).
[29] K. Helmerson, A. Martin, and D. Pritchard, J. Opt. Soc. Am. B **9**, 1988 (1992).
[30] P. Schmidt *et al.*, J. Opt. Soc. Am. B **20**, 960 (2003).
[31] P. Spoden *et al.*, Phys. Rev. Lett. **94**, 223201 (2005).
[32] C. Monroe *et al.*, Phys. Rev. Lett. **70**, 414 (1993).
[33] M. Arndt *et al.*, Phys. Rev. Lett. **79**, 625 (1997).
[34] S. Hopkins *et al.*, Phys. Rev. A **61**, 032707 (2000).
[35] G. Kavoulakis, C. Pethick, and H. Smith, Phys. Rev. A **61**, 053603 (2000).